Journal of Applied Physics

UV-black rutile TiO_2: An antireflective photocatalytic nanostructure

Cite as: J. Appl. Phys. **117**, 074903 (2015); https://doi.org/10.1063/1.4913222
Submitted: 06 December 2014 . Accepted: 07 February 2015 . Published Online: 20 February 2015

Ruy Sanz, Lucia Romano, Massimo Zimbone, Maria Antonietta Buccheri, Viviana Scuderi, Giuliana Impellizzeri, Mario Scuderi, Giuseppe Nicotra, Jens Jensen, and Vittorio Privitera

UV-black rutile TiO_2: An antireflective photocatalytic nanostructure

Ruy Sanz,[1,a)] Lucia Romano,[2] Massimo Zimbone,[1] Maria Antonietta Buccheri,[1] Viviana Scuderi,[1] Giuliana Impellizzeri,[1] Mario Scuderi,[3] Giuseppe Nicotra,[3] Jens Jensen,[4] and Vittorio Privitera[1]

[1]*CNR-IMM, Via Santa Sofia 64, I-95123 Catania, Italy*
[2]*Department of Physics, University of Catania, Via Santa Sofia 64, I-95123 Catania, Italy*
[3]*CNR-IMM, Zona industriale strada VIII n.5, I-95121 Catania, Italy*
[4]*Department of Physics, Chemistry and Biology, Linköping University, Linköping SE-581 83, Sweden*

(Received 6 December 2014; accepted 7 February 2015; published online 20 February 2015)

This work presents an experimental study on the specific quantitative contributions of antireflective and effective surface areas on the photocatalytic and antibacterial properties of rutile TiO_2 nanospikes. They are studied when continuously distributed over the whole surface and when integrated into well-defined microstructures. The nanospikes were produced following MeV ion beam irradiation of bulk rutile TiO_2 single crystals and subsequent chemical etching. The ion beam irradiation generated embedded isolated crystalline nanoparticles inside an etchable amorphous TiO_2 layer, and nanospikes fixed to the not etchable TiO_2 bulk substrate. The produced nanospikes are shown to resist towards aggressive chemical environments and act as an efficient UV antireflective surface. The photocatalytic activity experiments were performed under the ISO 10678:2010 protocol. The photonic and quantum efficiency are reported for the studied samples. The combined micro- and nanostructured surface triples the photonic efficiency compared to the initial flat surface. Results also revealed that the antireflective effect, due to the nanostructuring, is the dominating factor compared to the increase of surface area, for the observed photocatalytic response. The obtained results may be taken as a general strategy to design and precisely evaluate photoactive nanostructures. © *2015 AIP Publishing LLC*.
[http://dx.doi.org/10.1063/1.4913222]

I. INTRODUCTION

The optimization of the photocatalytic properties of TiO_2 based materials has been a focus of interest for the last 40 years,[1] due to their importance in clean energy and water remediation[2] systems. Several routes have been followed to increase the TiO_2 photoactivity, either by increasing the active surface area, e.g., through the creation of nanostructures, or modifying the band-gap in order to effectively use the visible part of the solar spectrum.[3] It is generally accepted that amorphous TiO_2 does not present any photocatalytic properties and that the anatase TiO_2 phase presents higher photo-catalysis yield than the more thermodynamic stable rutile TiO_2 phase.[4,5] However, three fundamental points are often neglected when discussing these materials: First, the long term stability or degradation under extensive cycles of use and/or application in aggressive environments; second, the efficiency in converting the incident light; and third, the effective or accessible surface area. Anatase dissolves in acid solutions at a faster rate[6] than the rutile phase and it suffers degradation under accelerated photocatalytic cycles,[7] and therefore its durability is compromised. The efficiency of collecting the incident light must be as high as possible, implying a low reflectance of the material. Although this issue is capital in other fields, e.g., in photovoltaic, where each reflected photon counts, only a few works have included or taken the effects of antireflective surfaces into account when studying photocatalytic applications of TiO_2.[8–12] Obviously, the variation of the reflectance modifies notably the overall photocatalytic yield of the materials, and should therefore be accounted for when comparisons between different materials are made. Differences in intrinsic properties of the material, i.e., band-gap modification, or extrinsic effects, such as surface topography, should also be pointed out.[13]

Sub-wavelength nanostructures, such as nanopores,[8] nanowires,[9] and hierarchical structures[12] offer advantages in terms of antireflective effects and are ideal to enhance the surface area for catalytic reaction. Although it is commonly assumed that the entire nanostructured surface is accessible to the used reactants, this point is not so obvious. Different molecules interact, and are adsorbed by the nanostructured surfaces, in distinct ways. As a result, a nanostructured surface may present different apparent photocatalytic yields depending on the type of photoreaction application studied, e.g., hydrogen generation or decomposition of organic pollutants in water. In a similar way, a major aspect for the practical application of TiO_2 for water remediation is the bactericide level of TiO_2 nanostructures, which is mainly governed by the photocatalytic generation of reactive oxygen species (ROS)[14] and the inflection of deformational stresses.[15] These effects are considered independent, but influencing the bio-fouling response. Finally, the selection

[a)]Author to whom correspondence should be addressed. Electronic mail: ruy.sanzgonzalez@cnr.it.

and design of a surface for being used as a photocatalytic material will often be a trade-off between durability, reactivity, and antibacterial capabilities.

This work reports a study concerning the contributions affecting the photocatalytic and antibacterial properties of ion-beam synthesized rutile TiO_2 nanostructures. The rutile TiO_2 phase was chosen in this work because of its long term chemical stability compared to the anatase phase.

II. EXPERIMENTAL

The employed process in this study for creating nanostructured surfaces is based on material modification by so-called ion track formation using swift heavy ion (SHI) irradiation and the subsequent chemical etching of the damaged material.[15,16] SHI irradiation may be used as a lithographic technique when applied together with suitable masks. In this way, the patterning of rutile TiO_2 single crystals has been successful in replicating micro-[17] and high aspect ratio nanostructures over cm^2 areas by using self-ordered porous alumina,[18–20] and colloidal microspheres as masks.[21,22]

The studied substrates were rutile TiO_2 $\langle 001 \rangle$ single crystals, $\approx 0.5 \times 0.5\,cm^2$, 0.5 mm thick, cut from the same $1 \times 1\,cm^2$ substrates, two side optical polished, with nominal RMS roughness of 0.2 nm, $\rho = 4.26\,g\ cm^{-3}$ (MTI corporation). In addition to inducing a needle-like (nanospikes) nanostructured surface on the initial flat rutile TiO_2, we also created nanospikes within a well-defined microscopic pattern using the lithographic capacities of the SHI process. The expected role of the microscopic pattern is to further increase the surface area, but at a different length scale than the over-laying nanostructure. For this, we employed colloidal silica microspheres $0.49 \pm 0.03\,\mu m$ in diameter (Duke Scientific Corporation) as a mask. This diameter of the colloids offered a microstructure with increased length scale compared to nanospikes. The colloidal masks were created by a self-organizing process.[21,22] In order to obtain a single layer of self-ordered silica microspheres, the TiO_2 substrates where exposed to UV light for 1 h. After this period, the exposed TiO_2 surfaces thereby become hydrophilic.[23,24] A colloidal microspheres solution was directly deposited onto the substrates and left dry under standard laboratory conditions until complete evaporation of water. This resulted in TiO_2 substrates covered with a mask consisting of a hexagonal closed packed (HCP) layer of colloidal micro-spheres, as shown in Fig. 1.

The two types of samples, bare rutile single crystals and covered by 0.5 μm in diameter colloids masks, were ion beam irradiated under the same conditions using 25 MeV Br^{+7} ions and a fluence of $1 \times 10^{14}\,cm^{-2}$ ($I > 50$ nA), at the Centro de Microanálisis de Materiales de Madrid. The expected projected ion range of Br ions under these conditions is $4.5 \pm 0.3\,\mu m$ (SRIM2013 code[25]), so that the atomic composition of the near-surface layer is not modified, and doping effects are consequently of minor importance. In addition, compared to conventional keV ion implantation energy, where collisional sputtering may induce changes in the surface stoichiometry of TiO_2,[26,27] compositional modifications are very small when using MeV ion energies. In order to complete the patterning process, all the irradiated TiO_2 samples were chemically etched in a 30% HF solution for 25 min to dissolve the ion beam created top layer of amorphous TiO_2.[17–22]

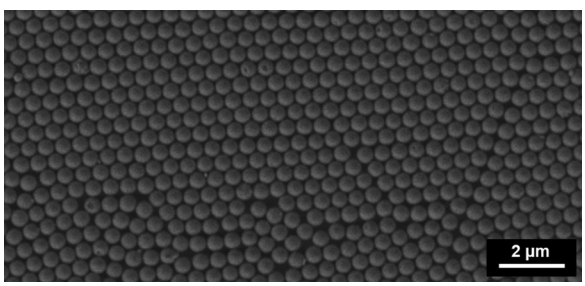

FIG. 1. SEM image of the silica colloid mask on the TiO_2 substrate before the ion beam irradiation process.

The surfaces of the irradiated and etched samples were characterized by FE-SEM (Carl Zeiss SUPRA 25) in plane and 45°-tilted view. TEM analysis of the samples was performed by using a JEOL ARM200CF with a cold FEG electron gun at a primary beam energy of 200 keV, operating in Conventional TEM (CTEM) and diffraction mode.

Total reflectance characterization (UV-vis) of the samples was measured by employing a spectrophotometer (Lamda45, Perking-Elmer) implemented with an integrating sphere (RSA-PE-20, Perking-Elmer).

The employed UV source (TL 8W BLB 1FM, Philips), for antibacterial and photocatalysis experiments, had an emission centered at a wavelength of 368 nm. The optical irradiance of the UV light at the given position on the surfaces of the samples was $1.1 \pm 0.1\ mW\ cm^{-2}$ in both type of experiments.

The antibacterial activity of our samples was tested on *Escherichia coli* (*E. coli*) ATCC 25922. *E. coli* is a well-known Gram-negative bacteria representative of coliforms, and considered as an indicator of faecal contamination. Hence, *E. coli* has been chosen as a model organism to evaluate the bactericidal activity of the samples by the colony-forming unit (CFU) method. A single colony was inoculated in 50 ml of Luria-Bertani (LB) broth and grown overnight at 37 °C by constant agitation at 180 rpm under aerobic conditions. The following day, the bacterial growth was measured by optical density at 600 nm. Bacteria were diluted up to 10^5 CFU/ml in phosphate buffer saline (PBS) and 100 μl were added onto the samples and subsequently exposed to UV. The untreated bacteria and bacteria exposed only to UV (not in contact with the TiO_2 samples) were investigated in parallel as controls. Experiments were made in triplicates. Aliquots were collected at 15, 30, and 60 minutes, respectively, conveniently diluted by serial dilutions 1:10 and plated in LB Agar Petri dishes. Plates were incubated overnight at 37 °C. CFU were counted the following day.

In order to evaluate the photocatalytic properties of the rutile TiO_2 surfaces, we followed the method given by the international standard ISO 10678:2010.[28,29] Other methods can effectively be applied, will however yield different results depending on the employed reactant.[30] The standard method used here is accepted by industry and assures a reliable measurement and identification of the various processes, i.e., adsorption, photo-bleaching, and photocatalysis, involved when a reactant, in this case the methylene blue

(MB), interacts with a photocatalytic surface under UV illumination. Preconditioning processes were applied, which included an initial UV illumination, using the same UV lamp and intensity mentioned above, for two hours to remove possible adsorbed organic pollutants on the surfaces,[24,29] allowing clean surfaces to absorb the MB molecules. Although this step is critical importance, several results in the literature omit this step with the risk of biasing the results. The cleaned samples were immersed in MB solutions and kept in dark for 12 h in order to evaluate the adsorption of MB on the different surfaces without involving photocatalytic reaction. After the MB adsorption step, the samples immersed in MB were exposed to UV to induce the photocatalytic reaction. The concentration of MB were monitored at several time intervals for both adsorption and photocatalytic process. The concentrations of the reactant during the measurement were extracted from the optical absorption spectra (664 nm)[28,29] employing the same spectrophotometer mentioned above.

After completed experiment, the samples were going through a cleaning process before being reused. They were exposed to UV light for 2 h in a de-ionized water bath and keep stored under standard atmospheric conditions. Three successive experiments of bactericidal and photo-catalytic activity were carried out by employing the same samples and experimental conditions with one week of spacing between experiments yielding similar results.

In addition, three supplementary experiments on the chemical resistance were performed by exposing the samples to H_2SO_4 (98 wt. %), HF (49 wt. %), and H_2O_2:H_2S0_4 (20:80) for 30 min, respectively. We did not detect any degradation in morphology or photocatalytic yield within the experimental error for all the structured TiO_2 samples after and before the etching baths. The chemical stability against aggressive etchants reinforces the confidence on the repeatability of the experimental results, endorsing the election of the created nanostructures as models for this study.

III. RESULTS AND DISCUSSION

A. Structure characterization

TEM analysis revealed the existence of a 1.4 μm thick amorphous layer of TiO_2 after the ion irradiation of the non-covered sample. Bright field (BF) TEM image in Fig. 2(a) shows isolated crystalline particles at the bottom of the amorphous layer, having a maximum diameter and length of 15 and 25 nm, respectively. They are close to a continuous acicular or nanospiked layer of damaged crystalline rutile. Selected area electron diffraction (SAED), Fig. 2(b), from isolated nanoparticles and acicular layer showed the same crystallographic orientation than the original substrate without the detection of grain rotation effects,[31] which has been reported at higher ion irradiation fluences. Nonetheless, both the isolated particles and the acicular layer present a damaged crystal lattice. The total damaged rutile layer, including the amorphous and acicular zone, extends down to 2150 nm from the original surface, as depicted Fig. 2(c). These differentiated structures originate in the mechanisms of energy transfer by the swift heavy ions to the crystal lattice in their path through the target. The 25 MeV Br ions transfer initially main part of their energy via inelastic interactions with the electronic cloud. Although this transfer of energy is below the reported threshold to generate isolated ion tracks in TiO_2 rutile single crystals,[32] the applied ion fluence allows the overlapping of defects created by individual ions along their trajectory in the sample. This damage formation by a collective effect results in a full amorphization of the single crystalline lattice, as given by, e.g., the exciton model.[33] Since the Br ions slow down along their path through the TiO_2, they eventually reach an energy close to the threshold to induce amorphization collectively, which corresponds to an electronic stopping power between 6.2 and 5.1 keV nm^{-1}[17,19] depending on the irradiation parameters. We will refer this region in the material as a transition region at the bottom of the amorphous zone. In this transition region, the stochastic fluctuations of energy and in the overlapping of ion trajectories determine the generation of a non-continuous amorphous volumes. As a result, different nanostructures form at the transition region: crystalline nanoparticles within the complete amorphous layer, where the fluctuations are able to inhibit the amorphization only in isolated volumes, and crystalline nanospikes where the fluctuations completely inhibit the continuum amorphization along the ion paths. It is clear that the mechanisms responsible for the observed nanostructures deserve a more detailed study, however, this is out of the scope of the present work.

After the HF chemical etching process, TEM analysis of the samples was performed again (Fig. 3). HF dissolved the

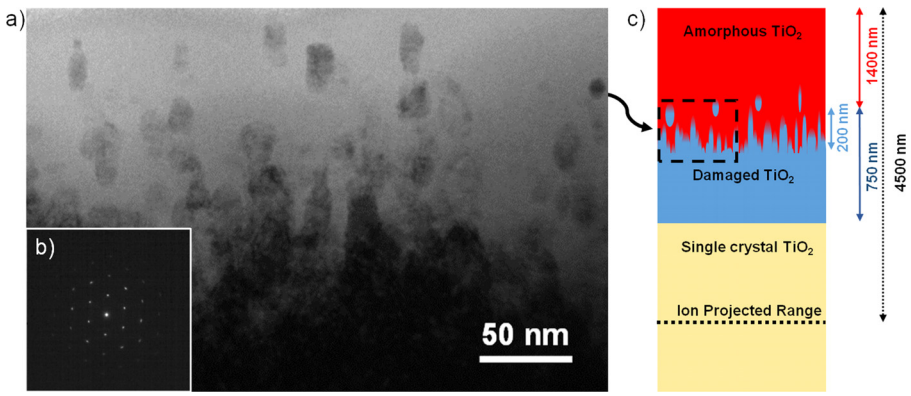

FIG. 2. (a) BF TEM image of crystalline TiO_2 nanoparticles and nanospikes surrounded by amorphous TiO_2 after SHI irradiation of rutile TiO_2 crystal. (b) SAED pattern of the nanospikes and damaged area. (c) Diagram of the different structures and composition of the sample after SHI irradiation.

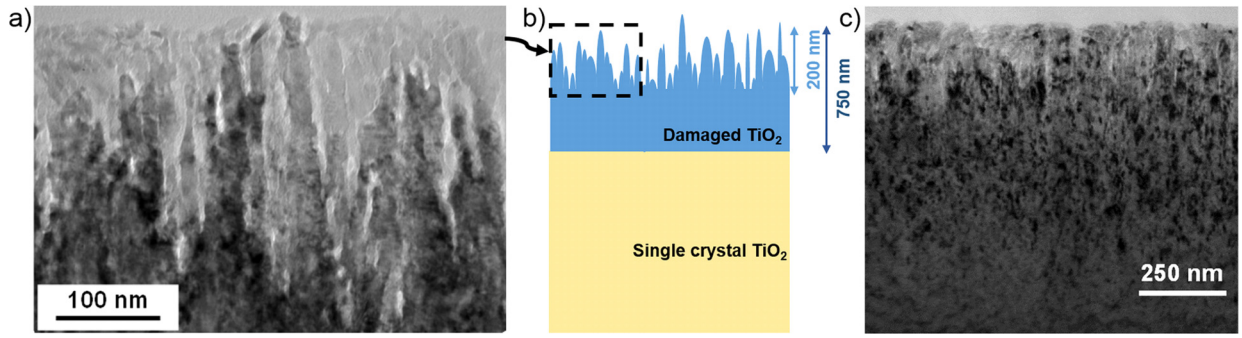

FIG. 3. TEM images of the irradiated and HF etched TiO_2 samples. (a) BF TEM image of the nanospikes. (b) Diagram of the different structures of the sample after the etching. (c) TEM image in two beam condition of the irradiated and etched samples showing the extension of the damaged area.

amorphous layer and the embedded nanoparticles disappeared. No detection of nanoparticles is justified by the fact that they were not retained after the dissolution of the surrounding amorphous layer matrix. The resulting surface appears only to be composed by TiO_2 nanospikes. These nanospikes have a maximum diameter of 30 nm and an average height of 200 ± 20 nm as measured by BF TEM imaging (Fig. 3(a)), in agreement with previous results.[34] Fig. 3(b) represents a schematic of the created structures. SAED from the nanospikes revealed that the nanospikes presented the same crystal orientation as the original single crystal. TEM image in two beam condition (Fig. 3(c)) shows, however, a damaged crystalline lattice. The total average thickness of the damaged rutile layer, including the nanospikes, is 750 ± 30 nm.

The surfaces of the irradiated and subsequent etched samples were examined by FE-SEM, and images are reported in Fig. 4. The samples irradiated without the colloidal mask presented a continuum of nanostructured surface of nanospikes (Fig. 4(a)). The samples irradiated through the colloid mask and etched represent a projection of the colloid microspheres onto the surface[21,22] (Fig. 4(c)). The resulting 0.5 μm TiO_2 hemispheres are arranged in HCP order overlaid by the nanostructure. The surfaces of the obtained hemispheres and the areas between them exhibit a similar nanospike structure (Fig. 4(d)) as seen on the samples irradiated without mask. Thus, we assume that the nanospiked surface having a HCP microstructure order should present the same characteristics as the continuum nanostructured surface under the current patterning conditions.

Regarding the expected increase of the surface area by the HCP microstructure, it is important to note that the ratio between the surface areas of an perfect HCP array of hemispheres and a flat surface is $(\pi/2 + \sqrt{3})/\sqrt{3}$ (≈ 1.91), this ratio being independent of the diameter of the considered hemispheres. A perfect homogeneous long-range HCP arrangement was unfortunately not obtained (Fig. 4(c)). Different forces between particles and the pilling-up of two or more layers of silica microspheres caused the distortions in the HCP ordering (Fig. 1).[21,22] Although some distortions decrease the resulting surface area, other may increase it, i.e., those obtained by pilling-up of colloids in different layers. Therefore, the exposed surface areas for these samples may slightly differ from the theoretical value.

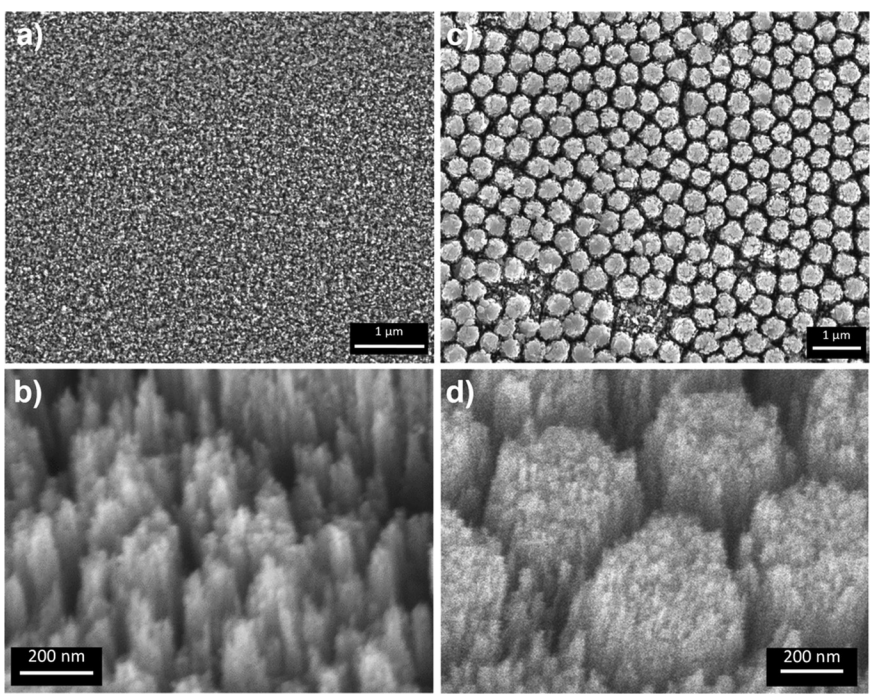

FIG. 4. SEM images from TiO_2 surface after SHI irradiation and HF etching. (a) The obtained nanospikes on the bare substrate. (b) Detailed tilted image from a). (c) HCP hemispheres replica images (top-view). (d) Detailed tilted image from c).

B. Optical characterization

The total reflectance of the nanostructured samples exhibits an almost completely suppression, <2%, of the reflectance in the range from 300 to 410 nm and a 50% decrease in the range from 410 to 700 nm compared to the original rutile single crystal (Fig. 5). Murphy[13] previously reported this decrease in the reflectance for 1 μm thick TiO_2 layers, with a RMS roughness of 10 nm, exclusively due to a topography related phenomena and not due to a band-gap modification. Similar nanospike structure is also present on so-called black silicon,[14] and in TiO_2 nanowires composed of mesocrystals,[12] where the antireflection effect can be explained in terms of an effective refraction index.[35] By analogy, in the present case, we can talk about UV-black TiO_2. It is also noticeable that recent work[26] reports anomalous optical adsorption phenomena, up to 60%, on oxygen defective nanostructured (15 nm diameter, 0.5 nm height) surfaces created using low energy 60 keV Ar^+ bombarded rutile TiO_2. In addition to the observed suppressed reflectance on our samples, three details stand out. First, all SHI irradiated samples present the same characteristic band-gap edge of rutile TiO_2 (410 nm), in spite of the damaged crystalline structures that might shift the band-gap edge. Second, when the reflectance of both types of structured samples is compared, there is no difference in the 300–410 nm region, pointing to the predominance of the antireflective effect of the nanostructure versus the HCP microstructure. And third, the reflectance of the HCP replica is slightly higher than the continuum surface of nanospikes for wavelengths larger than 410 nm. It is worth to note that the emission spectra of the employed UV light for the photocatalytic and antibacterial studies, also represented in Fig. 5, fall into the maximum suppressed range of wavelengths.

C. Antibacterial activity

Results of antibacterial activity are presented in Fig. 6. After one hour of exposure to UV, the *E. coli* survival percentage had reduced to ~65% on the flat rutile single crystal whereas in same period, the survival percentage of *E. coli* in contact with the nanospikes and the HCP pattern samples is

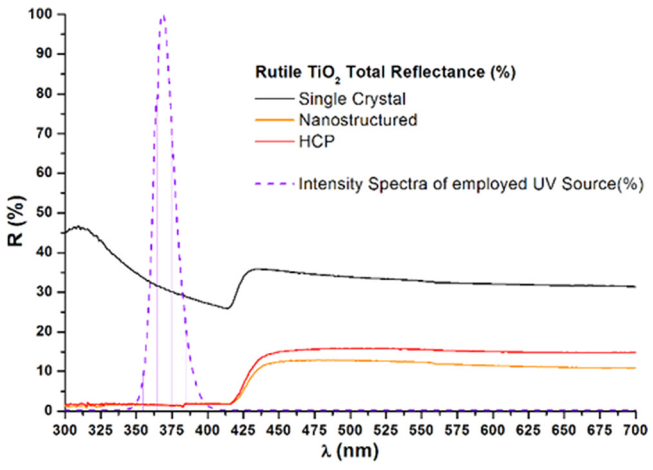

FIG. 5. Reflectance spectra from TiO_2 with different surface morphology and the UV intensity spectra of the employed light source.

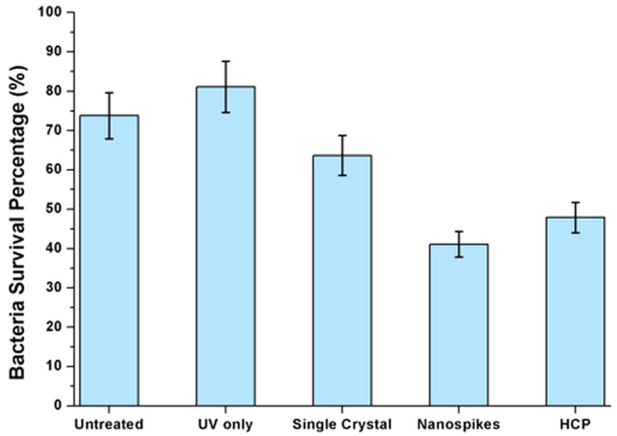

FIG. 6. Bacteria survival percentage on the studied TiO_2 surfaces after one hour to UV exposure.

reduced to 41% and 47%, respectively. Hence, the nanospikes and HCP patterns show similar antibacterial activity, which is higher if compared to the efficiency showed by a flat single crystalline samples. Exposure of *E. coli* to UV light in the absence of TiO_2 reduced the bacteria survival percentage only to 85%, thus damage due to UV light only is modest. Therefore, the major reason for the antibacterial effect is due to the additional presence of TiO_2 nanostructures. As shown in Fig. 5, both samples with a nanostructured surface display an enhanced antibacterial activity compared to the flat surface, indicating that elongated nanostructured materials effectively result in an improvement. This therefore suggests that, with regard to antibacterial activity, the two surface model structures may be equally implemented.

It is generally accepted that TiO_2 based nanomaterials show an antibacterial effect through a mechanism of oxidative stress due to ROS that are generated in the UV/TiO_2 process in an aqueous environment, where the hydroxyl radical being mainly responsible for *E. coli* inactivation.[14] The inflection of deformational stresses is believed to be the main expected antibacterial effect of elongated nanostructured surfaces.[15] This shape-related effect appears independent of the biochemical functionality, which is mainly governed by the photo-generated ROS. Leaving beside the possible interactions of bacteria with the surfaces, the deformational stresses are likely to be of similar magnitude for both type of nanostructured samples and it is therefore reasonable that a higher generation of ROS on nanostructured surfaces is responsible for the observed stronger antibacterial effect. However, from the results in this biological experiment is not possible to assess the quantitative photocatalytic yield of the nanostructured surface.

D. Photocatalytic activity

No degradation of MB control solutions (photo-bleaching without contact to the TiO_2 samples), under same UV exposure conditions, was detected in parallel experiments. Furthermore, the photoactivity of the as-irradiated samples, but not chemically etched, was also evaluated by following the same method. Here, no photocatalytic yield was

observed, which suggest that the amorphous layer induced by the SHI does not present any photoactivity, which has been observed before,[4,5] or that the yield is below the detection threshold under the employed measurement conditions. Therefore, the results from this type of sample will not be presented here.

Results from the measurements of the photocatalytic activity of the structured are presented in Fig. 7. The optical absorbance of the MB solution, and thus its concentration,[28,29] is presented in Fig. 7(a), where error bars include instrumental and statistical errors. The "dark" denoted time range refers to the variation of concentration of MB in dark conditions. Therefore, the subsequent measured variations in concentration were only due to different amount of initial adsorbed MB on the surfaces of the samples. The results show that the main amount of MB adsorbed on the sample surfaces takes place within the first 40 min. The adsorbed amount of MB after 12 h is similar (<1%) to that at 40 min, and thus we can assume that the surfaces have reached a steady-state of adsorption after 12 h. The adsorbed amounts of MB were calculated by normalizing to the samples' macroscopic areas as reported in Table I. The adsorbed amount of MB per macroscopic area of all the patterned samples was 30% higher than that of the flat rutile. The differences between patterned samples are within the experimental error.

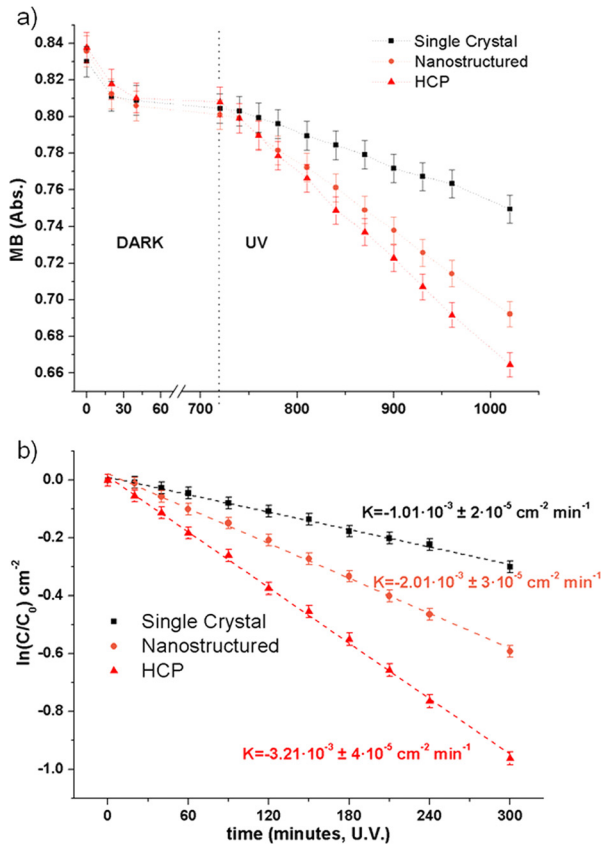

FIG. 7. (a) Absolute optical absorbance (concentration) of methylene blue solutions at 664 nm measured during the photocatalysis experiments on the studied TiO_2 surfaces (lines are only for eye guide). (b) Time dependence in the steady-state photocatalytic regime of the logarithmic normalized concentration. Note that the values have been normalized to the macroscopic area of each sample.

The "UV" denoted plotted area in Fig. 7(a) refers to the variation of the MB concentration in UV illumination conditions. Since the surfaces were previously saturated with MB molecules, and no photo-bleaching of the molecules on the control solution was detected, we assume that the decay in MB concentration is only related to degradation of the reactant through a photocatalytic reaction with the surface. A pseudo-first order photocatalytic rate constant, K (Table I), was extracted from steady state photocatalytic regimes, and normalized to macroscopic surface area (lines in Fig. 7(b) represent fitting). The mean photonic efficiencies of MB degradation, ζ_{MB} (Table I), were calculated following the method described in Ref. 29. Both the photocatalytic rate constants and ζ_{MB}, with respect to the flat single crystal, increased by a factor of two and three for the nanostructured and HCP patterned samples, respectively (Table I). The quantum efficiencies,[36] Φ (Table I) were calculated considering the integration of the total reflectance spectra of the samples within the range of the employed UV light source spectra (Fig. 5). These values allow to calculate the efficiency of the incident or adsorbed photons employed in the degradation of MB. Please note that to ease comparison we express both efficiencies in %, ζ_{MB} refers to the total incident light and, Φ only refers the adsorbed photons (in this case, not reflected). It is also worth to note that reported ζ_{MB} of a commercial self-cleaning and photocatalytic glass is in the order of 0.025%.[37]

In order to analyze the obtained apparent photocatalytic yield of the samples, it is necessary to take into account different factors that influence the reaction. The active surface areas for the photocatalytic reaction are different for each type of sample. The reaction rate enhancement of the HCP replica surface with respect to the simple nanostructured surface is scaling in accordance with the predicted increase in surface area. In fact, the theoretical increase in surface area for HCP is 1.91 times compared to that without HCP patterning and the photocatalytic yield of HCP replica is 1.6 higher than for the simple nanostructured surface. This reduction of 16% with respect to the ideally expected value is probably due to the distortion in the ordering of the micro-pattern. However, this approach is not verified when comparing the nanostructured surface with that of flat rutile surface. The nanostructured surface with respect to the untreated rutile sample can be roughly morphologically modelled as a close packet array of nanocylinders with the size measured by TEM. This gives an ideal increase in the surface area of the nanostructure with respect to the flat sample of a factor 24 (Table I). Nonetheless, the photocatalytic rates do not reflect this increase of one order of magnitude predicted for the nanostructures. Although, the dynamic mechanisms of liquid circulation around[38] and inside nanostructures are not obvious,[39,40] and considering the experimental data, it is plausible that the liquid circulation, or the access to the surfaces, are not affected at the microscale, but are hampered at the nanoscale.

Thus, we should first analyze the initial interaction of MB with the nanostructure. The applied method to measure the photocatalytic yield gives an approximate evaluation of the adsorbed amount of reactant on the clean surfaces after

TABLE I. Photocatalytic and surface area results for the three studied surface structures.

	Single crystal	Nanospike	HCP
Adsorbed MB (μmol cm^{-2})	$3\times10^{-3}\pm2\times10^{-3}$	$4\times10^{-3}\pm2\times10^{-3}$	$4\times10^{-3}\pm2\times10^{-3}$
K (cm^{-2}min^{-1})	$-1.01\times10^{-3}\pm2\times10^{-5}$	$-2.01\times10^{-3}\pm3\times10^{-5}$	$-3.21\times10^{-3}\pm4\times10^{-5}$
ζ_{MB} (%)	0.010 ± 0.002	0.019 ± 0.002	0.031 ± 0.004
Φ (%)	0.014 ± 0.003	0.020 ± 0.002	0.031 ± 0.004
Theoretical estimation of normalized surface area	1	24[a]	46[b]

[a]Calculated assuming hexagonal close packet nanocylinders.
[b]Includes the HCP hemispheres ratio.

the previous irradiation with UV light. Increments in the adsorbed amount of reactants during the initial dark range should be directly related to the increased available or active surface areas for molecules. These active surface areas may not correspond to those obtained by standard BET measurements of specific surface area[35] since the adsorbed species are different. Although a slight increased amount of adsorbed MB in nanostructured samples was detected, this was far from the increase of one order of magnitude seen for the surface area. Nonetheless, another not evident possibility may determine the access of MB to the nanostructures. A TiO_2 surface exposed to standard atmosphere adsorbs spontaneously hydrocarbon species. The illumination with UV eliminates these species from the surface, and as a result a hydrophilic and clean TiO_2 surface is obtained[36] However, the antireflective effect of the nanospikes could indicate a complete adsorption of photons in the first nm of the nanostructured layer. Therefore, the removal of the previously adsorbed hydrocarbon species in the deeper surface zones of the nanospikes would not take place, and thus hinder the absorption of MB.

In spite of the limited information regarding the adsorption process that can be extracted with the employed method, and therefore about the active surface areas, the reported increases in photocatalytic activity are quantitatively below the increase of one order of magnitude that was expected if the whole area of the nanostructured surface was accessible to the reactant (MB). Therefore, no clear evidences support that the whole surface area of the nanostructure offers an increased active surface for the present photocatalytic degradation of an organic molecule.

We should also note that besides the differences in available effective surface area for the reaction, the samples also exhibit different efficiencies collecting photons. The enhancement in the light trapping efficiency will provide additional photo-generated carriers, and evidently an increased photocatalytic activity. However, intrinsic variation in the reactivity of the nanospikes due to crystalline damage, different crystalline surfaces,[41] and local variations of stoichiometry[42,43] should also be taken into account. If an increase in the number of harvesting photons is responsible for the observed enhanced photoactivity of nanospikes, then correcting the obtained Φ value from the flat sample, with the observed effect of the increased surface area from the nanospikes, measured by the MB adsorption, should give a corrected Φ value for the flat sample similar to that for nanostructured. Applying this correction to the Φ for the flat sample, a value of 0.0186 is obtained, which is close to the Φ value of 0.020 obtained from the nanospike samples. The same conclusion can be drawn for the HCP replica patterned sample within the experimental error. Although these corrected values of Φ can be affected by an intrinsic variation in the reactivity of the nanospikes, such effects seem to be minimum in the present case.

Nonetheless, recent results show that only carriers generated in the first nanometers surface layers of bulk rutile TiO_2 contribute to the photoreaction.[5] If similar lifetimes for the photo-generated electron-hole pairs[43] are considered for bulk and nanostructured rutile, then the reduced size of the nanospikes should increase the probability of carriers to avoid recombination and reach the surface. This could explain net positive effect in the observed Φ from the nanostructures, which is compatible with the obtained photocatalytic yields, the optical properties and the limited active surface area.

IV. CONCLUSIONS

The ion irradiation of rutile single crystal TiO_2 substrates with 25 MeV Br ions at a high fluence generates an amorphous TiO_2 layer with embedded crystalline nanoparticles and nanospikes. Removing the amorphous material by subsequent HF etching results in a surface consisting of TiO_2 nanospikes standing on the rutile substrate. Although the nanospikes present crystalline defects due to the irradiation process, they did not degrade their qualities after exposure to extreme solutions. They exhibit an enhanced antibacterial and photocatalytical activity compared to flat rutile TiO_2 surfaces and commercial available photoactive glasses. The presented results reveal that the most important effect of the generated nanospikes on a rutile TiO_2 surface is the suppression of reflectance, particularly in the UV range of the spectra. By comparing with black silicon, we can here talk of UV-black TiO_2. When integrating the nanospikes into a HCP microstructure, the surface area increases and also the observed photocatalytic yield without varying the antireflective efficiency in the UV range. We did not detect any evidence of an effective full penetration of the reactant (MB) between the nanostructures.

The present work highlights the complex characterization of the photocatalytic and antibacterial activity of nanostructures, where many factors—optics, reactivity, and effective exposed surface—have to be taken into account when nanostructures are coming into play with respect to flat surfaces. It may serve as an example of how a nanostructured

surface may enhance the reaction efficiency without decisive variation of its chemical composition, merely by enhancing the efficiency of its optical properties and integrating them into a proper microstructure. The importance to obtain high aspect-ratio nanostructures for photocatalytic processes should therefore be carefully evaluated and balanced accordingly in future material designs.

ACKNOWLEDGMENTS

We acknowledge the support of the European Commission by the FP7 WATER project (Grant agreement 316082), of the Italian Ministry of Education and Research by the project Beyond-Nano (PON a3_00363). J.J. thanks the Carl Tryggers Foundation and the VR Linnaeus grant LiLi-NFM for financial support. Authors are grateful to Professor Stefania Stefani, Laboratory of Medical Microbiology and Antibiotic Resistance (MMAR), Università di Catania, Italia, for the *Escherichia Coli* strain and for useful discussions.

[1]A. Fujishima, X. Zhang, and D. A. Tryk, Surf. Sci. Rep. **63**, 515 (2008).
[2]X. Qu, J. Brame, Q. Li, and P. J. J. Alvarez, Acc. Chem. Res. **46**, 834 (2013).
[3]R. Daghrir, P. Drogui, and D. Robert, Ind. Eng. Chem. Res. **52**, 3581 (2013).
[4]M. Xu, Y. Gao, E. Martinez Moreno, M. Kunst, M. Muhler, Y. Wang, H. Idriss, and C. Wöll, Phys. Rev. Lett. **106**, 138302 (2011).
[5]T. Luttrell, S. Halpegamage, J. Tao, A. Kramer, E. Sutter, and M. Batzill, Sci. Rep. **4**, 4043 (2014).
[6]T. Ohno, K. Sarukawa, and M. Matsumura, J. Phys. Chem. B **105**, 2417 (2001).
[7]L. Zhang, B. K. Miller, and P. A. Crozier, Nano Lett. **13**, 679 (2013).
[8]S. Guldin, P. Kohn, M. Stefik, J. Song, G. Divitini, F. Ecarla, C. Ducati, U. Wiesner, and U. Steiner, Nano Lett. **13**, 5329 (2013).
[9]H. J. Hwang, A. Boukai, and P. Yang, Nano Lett. **9**, 410 (2009).
[10]H. Li, B. Jiang, R. Schaller, J. Wu, and J. Jiao, J. Phys. Chem. C **114**, 11375 (2010).
[11]J. Cai, J. Ye, S. Chen, X. Zhao, D. Zhang, S. Chen, Y. Ma, S. Jin, and L. Qi, Energy Environ. Sci. **5**, 7575 (2012).
[12]A. Hu, R. Liang, X. Zhang, S. Kurdi, D. Luong, H. Huang, P. Peng, E. Marzbanrad, K. D. Oakes, Y. Zhou, and M. R. Servos, J. Photochem. Photobio. A **256**, 7 (2013).
[13]A. B. Murphy, Sol. Energy Mater. Sol. Cells **91**, 1326 (2007).
[14]M. Cho, H. Chung, W. Choi, and J. Yoon, Water Res. **38**, 1069 (2004).
[15]E. P. Ivanova, J. Hasan, H. K. Webb, G. Gervinskas, S. Juodkazis, V. K. Truong, A. H. Wu, R. N. Lamb, V. A. Baulin, G. S. Watson, J. A. Watson, D. E. Mainwaring, and R. J. Crawford, Nat. Commun. **4**, 2838 (2013).
[16]R. Spohr, *Ion Tracks and Microtechnology, Principles and Applications* (Vieweg & Sohn Verlagsgesellschaft mbH: Braunschweig, 1990).
[17]K. Nomura, T. Nakanishi, Y. Nagasawa, Y. Ohki, K. Awazu, M. Fujimaki, N. Kobayashi, S. Ishii, and K. Shima, Phys. Rev. B **68**, 064106 (2003).
[18]R. Sanz, A. Johansson, M. Skupinski, J. Jensen, G. Possnert, M. Boman, M. Vázquez, and K. Hjort, Nano Lett. **6**, 1065 (2006).
[19]R. Sanz, J. Jensen, A. Johansson, M. Skupinski, G. Possnert, M. Boman, M. Hernandez-Vélez, M. Vazquez, and K. Hjort, Nanotechnology **18**, 305303 (2007).
[20]R. Sanz, M. Jaafar, M. Hernández-Vélez, A. Asenjo, M. Vázquez, and J. Jensen, Nanotechnology **21**, 235301 (2010).
[21]J. Jensen, M. Skupinski, K. Hjort, and R. Sanz, Nucl. Instrum. Methods Phys. Res. B **266**, 3113 (2008).
[22]M. Skupinski, R. Sanz, and J. Jensen, Nucl. Instrum. Methods Phys. Res. B **257**, 777 (2007).
[23]R. Wang, N. Sakai, A. Fujishima, T. Watanabe, and K. Hashimoto, J. Phys. Chem. B **103**, 2188 (1999).
[24]J.-Y. Zheng, S.-H. Bao, Y. Guo, and P. Jin, ACS Appl. Mater. Interfaces **6**, 1351 (2014).
[25]See http://www.srim.org.
[26]V. Solanki, S. Majumder, I. Mishra, P. Dash, C. Singh, D. Kanjilal, and S. Varma, Appl. Phys. Lett. **98**, 053105 (2011).
[27]S. Hashimoto, A. Tanaka, A. Murata, and T. Sakurada, Surf. Sci. **556**, 22 (2004).
[28]H. M. Branz, V. E. Yost, S. Ward, K. M. Jones, B. To, and P. Stradins, Appl. Phys. Lett. **94**, 231121 (2009).
[29]*Fine ceramics (advanced ceramics, advanced technical ceramics) — Determination of photocatalytic activity of surfaces in an aqueous medium by degradation of methylene blue. ISO 10678:2010(E).* International Organization for Standardization (2010). Switzerland.
[30]A. Mills, C. Hill, and P. K. J. Robertson, J. Photochem. Photobiol. A. **237**, 7 (2012).
[31]M. Ishimaru, Y. Hirotsu, F. Li, and K. E. Sickafus, Appl. Phys. Lett. **77**, 4151 (2000).
[32]K. Awazu, X. Wang, M. Fujimaki, T. Komatsubara, T. Ikeda, and Y. Ohki, J. Appl. Phys. **100**, 044308 (2006).
[33]A. Rivera, M. L. Crespillo, J. Olivares, R. Sanz, J. Jensen, and F. Agulló-López, Nucl. Instrum. Methods Phys. Res. B **268**, 3122–3126 (2010).
[34]J. V. Pérez-Girón, M. Hirtz, C. McAtamney, A. P. Bell, J. A. Mas, M. Jaafar, O. De Luis, H. Fuchs, J. Jensen, and R. Sanz, Nucl. Instrum. Methods Phys. Res. B **339**, 67 (2014).
[35]J. Ryu and W. Choi, Environ. Sci. Technol. **42**, 294 (2008).
[36]N. Serpone and A. Salinaro, Pure Appl. Chem. **71**, 303 (1999).
[37]R. Fateh, R. Dillert, and D. Bahnemann, ACS Appl. Mater. Interfaces **6**, 2270 (2014).
[38]C. Sendner, D. Horinek, L. Bocquet, and R. R. Netz, Langmuir **25**, 10768 (2009).
[39]G. Shen, X. H. Zhang, Y. Ming, L. Zhang, Y. Zhang, and J. Hu, J. Phys. Chem. C **112**, 4029 (2008).
[40]B. Liu, K. Nakata, S. Liu, M. Sakai, T. Ochiai, T. Murakami, K. Takagi, and A. Fujishima, J. Phys. Chem. C **116**, 7471 (2012).
[41]A. Y. Ahmed, T. A. Kandiel, T. Oekermann, and D. Bahnemann, J. Phys. Chem. Lett. **2**, 2461 (2011).
[42]M. K. Nowotny, L. R. Sheppard, T. Bak, and J. Nowotny, J. Phys. Chem. C **112**, 5275 (2008).
[43]L. Liu, P. Y. Yu, X. Chen, S. S. Mao, and D. Z. Shen, Phys. Rev. Lett. **111**, 065505 (2013).